Numerical Study on Micropolar Nanofluid Flow over an Inclined Surface by Means of Keller-Box

Abstract

In this paper, Micropolar Nanofluid boundary layer flow over linear inclined extending surface with magnetic effect investigated. Model utilized in this examination depends on Buongiorno model for the thermal efficiencies of the liquid flow in the presence of Brownian movements and thermophoresis properties. The nonlinear problem for Micropolar Nanofluid flow over slanted channel is demonstrated to consider the heat and mass exchange marvel by considering portent flow parameters to strengthened boundary layers. The administering nonlinear partial differential equations are changed to nonlinear ordinary equations and a short time later outlined numerically by strategies for the Keller-Box plan. A correlation of the set up results in the absence of the incorporated impacts is performed with the accessible results and perceived in a decent settlement. Numerical and graphical outcomes are additionally exhibited in tables and diagrams.

Keywords: Micropolar Nanofluid, MHD, inclined surface.

1 Introduction

Nanofluids set up a subclass of sub-atomic liquids intended to work at the nanoscale. Nanofluids comprise connection between mass materials and sub-atomic structure. The quick advancement of nanotechnology has seen a critical consideration in such fluids through the entire expansiveness of assembling, including building, aviation, restorative creations and vitality innovations. Nanofluid is a blend of various nanoparticles, for example, aluminum, silver, copper and titanium with or without their oxides and base liquids including water, ethylene glycol and oil and so forth when nanoparticles deliberately scattered in the base liquids, the subsequent nanofluids have been affirmed to achieve critical enhancement in the properties of thermal conductivity, introduced by Choi [1]. The elements that play essential principle to upgrade the thermal conductivity of nanofluid has been considered by Buongiorno [2]. He found that the thermal conductivity of the fluid increment due to thermophoresis and Brownian movement impacts in the ordinary liquid. Brownian movement is the unpredictable development of the nanoparticles in the conventional liquid and caused the constant impacts between based liquid and nanoparticles. Thermophoresis is the wonder which diffuses the particles because of the temperature inclination. The heat transfer of nanofluid over a nonlinear porous

36 sheet is numerically discussed by Zaimi et al. [3]. Anwar et al. [4] contemplated
37 the numerical investigation of micropolar nanofluid flow over an extending sheet. Nanofluid
38 flow over a slanted extending surface concentrated by Sandeep and Kumar [5]. They researched
39 heat and mass exchange of dusty nanoparticles improved on account of the volume division of
40 nano particles. Suriyakumar and Devi [6] communicated the impacts of inner heat generation and
41 suction on blended convective nanofluid flow through slanted surface. Ziaei-Rad et al. [7]
42 examined the similarity solution of boundary layer nanofluid flow on an inclined surface.
43 Rashad [8] studied nanofluid flow by considering convective boundaries and anisotropic slip
44 effect. Mitra [9] investigated computational modeling of nanofluid flow over a heated inclined
45 plate. Khan et al. [10] outlined the heat and mass exchange of MHD Jeffery nanofluid flow over
46 slanted sheet. Hatami et al. [11] examined three dimensional relentless nanofluid over a slanted
47 plate.

48 The boundary layer flow over a slanted extending surface turn into an intriguing field of research
49 on account of its uses in building, for example, paper creation, skin rubbing, grain stockpiling
50 and drag generation. The investigation of boundary layer flow over ceaseless surface begun by
51 Sakiadis [12]. Also, Crane [13] examined the closed form arrangement of boundary layer flow
52 over an extending sheet. The boundary layer stream of dusty liquid over a slanted surface with
53 heat source/sink was introduced by Ramesh et al. [14]. Singh [15] explored heat and mass
54 exchange of thick liquid on porous slanted plate. Similarity solution of magnetohydrodynmaic
55 flow over a slanted sheet was examined by Ali et al. [16]. Ramesh et al. [17] took a shot at the
56 boundary layer flow over slanted sheet with convective limits. MHD free convection dissipative
57 liquid flow past over a slanted permeable surface was examined by Malik [18]. Hayat et al. [19]
58 investigated radiation effect on the flow induced by stretching cylinder by considering non-
59 uniform heat source/sink. Balla et al. [20] examined an inclined porous cavity filled with
60 nanofluid saturated in permeable medium.

61 Micropolar liquids are those, which contain unbending arbitrarily situated particles submerged in
62 a gooey medium with microstructure constituent, where bending of the molecule is unnoticed.
63 Eringen [21] built up another reasoning of micropolar liquid to check the impact of small scale
64 revolutions on smooth movement. Rahman et al. [22] talked about the flow of micropolar liquid
65 by thinking about the variable properties. Micropolar fluid flow by taking different effects over
66 an inclined sheet was studied by Das [23]. Kasim et al. [24] inspected the micropolar liquid flow
67 on the slanted plate numerically. Srinivasacharya and Bindu [25] researched micropolar liquid
68 move through a slanted channel having parallel plates. Hazbavi and Sharhani [26] analyzed the
69 flow of micropolar liquid between two parallel plates with steady weight slope. Shamshuddin et
70 al. [27] contemplated the heat and mass exchange of micropolar liquid flow through penetrable
71 slanted plate. The impact of two fold scattering on micropolar liquid flow over a slanted surface
72 was examined by Srinivasacharya et al. [28].

73 **2 Problem formulation**

74 A steady, two dimensional boundary layer flow of micropolar Nano fluid over a permeable
75 inclined linear stretching plate with an angle γ is considered. The stretching and free stream
76 velocities are supposed to be as, $u_w(x) = ax$ and $u_\infty(x) = 0$ respectively, here 'x' is the
77 coordinate dignified lengthways the enlarging surface and 'a' is a constant. An external
78 transverse magnetic field is taken normal to the flow path. It is supposed that the electric and
79 magnetic field effects are very minor as the magnetic Reynolds number is less, Mishra et al.
80 [29].The micropolar finite size particles along with Nano particles are constantly distributed in
81 the base fluids. The fluid particles have extra space to travel about formerly hitting to the other
82 fluid particle, where these particles revolve in the fluid field and fallouts for spinning effects in
83 the micropolar nanofluid. The Brownian motion and thermophoresis effects are taken into
84 account. The temperature T and Nano particle fraction C at the wall take the constant values T_w
85 and C_w, while the ambient forms used for nanofluid temperature and mass fractions T_∞ and C_∞
86 are attained as y lean towards to immensity shown in fig.1.
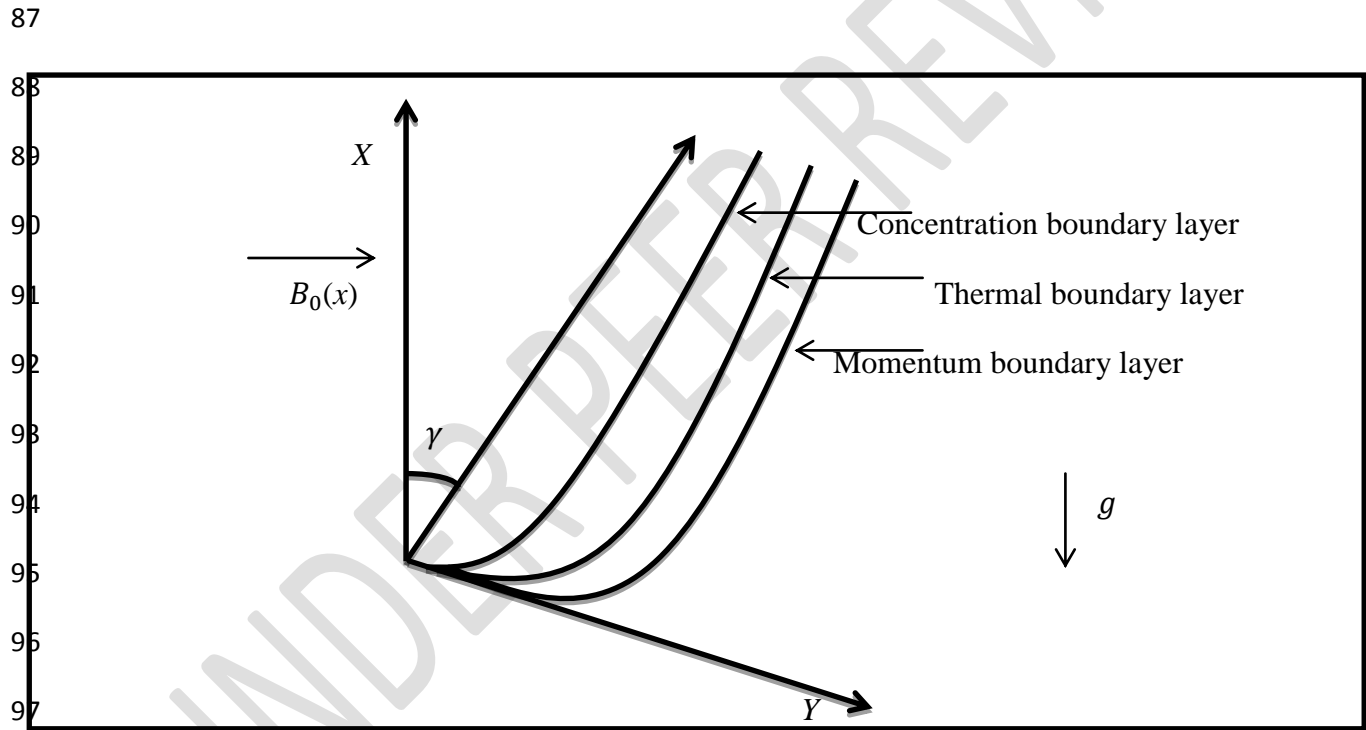
87

Fig.1. Physical geometry and coordinate system

101 The flow equations for this study are given by

103     $\frac{\partial u}{\partial x} + \frac{\partial v}{\partial y} = 0,$ (1)

104     $u\frac{\partial u}{\partial x} + v\frac{\partial u}{\partial y} = \left(\frac{\mu+K_1^*}{\delta}\right)\frac{\partial^2 u}{\partial y^2} + \left(\frac{K_1^*}{\rho}\right)\frac{\partial N^*}{\partial y} + g[\beta_t(T - T_\infty) - \beta_c(C - C_\infty)]cos\gamma - (\frac{\sigma B_0{}^2(x)}{\rho} + \frac{\mu}{\rho k})u,$ (2)

105     $u\frac{\partial N^*}{\partial x} + v\frac{\partial N^*}{\partial y} = \left(\frac{\gamma^*}{j^*\delta}\right)\frac{\partial^2 N^*}{\partial y^2} - \left(\frac{K_1{}^*}{j^*\delta}\right)\left(2N^* + \frac{\partial u}{\partial y}\right),$ (3)

106     $u\frac{\partial T}{\partial x} + v\frac{\partial T}{\partial y} = \alpha\frac{\partial^2 T}{\partial y^2} + \tau\left[D_B\frac{\partial C}{\partial y}\frac{\partial T}{\partial y} + \frac{D_T}{T_\infty}\left(\frac{\partial T}{\partial y}\right)^2\right],$ (4)

107     $u\frac{\partial C}{\partial x} + v\frac{\partial C}{\partial y} = D_B\frac{\partial^2 C}{\partial y^2} + \frac{D_T}{T_\infty}\frac{\partial^2 T}{\partial y^2},$ (5)

108   Where in the directions x and y the velocity constituents are u and v, individually, g is the
109   gravitational acceleration, the uniform magnetic field strength is given by B_0, σ denotes the
110   electrical conductivity, the viscosity is denoted by μ, the density of the base liquid is given by δ_f,
111   the density of the nanoparticle is given by δ_p, the vortex viscosity is defined as k_1^*, factor of
112   thermal increase is given by β_t, β_c denotes constant of concentration extension, the gyration
113   ascent viscosity is given by γ^*, the micro inertia of each mss component mass is given by j^*, the
114   micro-rotation is given by N^*, D_B denote the Brownian dispersal factor and D_T denotes the
115   thermophoresis dispersion amount, k is the thermal conductivity, the heat capacity of the
116   nanoparticles is denoted by $(\delta c)_p$, $(\delta c)_f$ represents the heat capacity of the conventional liquid,
117   thermal diffusivity parameter is denoted by $\alpha = \frac{k}{(\delta c)_f}$ and the relation among the active heat

118   capacity of the nanoparticle and heat capacity of the liquid is represented by $\tau = \frac{(\delta c)_p}{(\delta c)_f}$.

119   The subject boundary conditions are

120     $u = u_w(x) = ax, v = 0, T = T_w, N^* = -m_0\frac{\partial u}{\partial y}, C = C_w \quad at \quad y = 0,$

121     $u \to u_\infty(x) = 0, v \to 0, T \to T_\infty, N^* \to 0, \ C \to C_\infty \quad at \quad y \to \infty,$ (6)

122

123   The nonlinear ordinary differential equations are obtained from nonlinear partial differential
124   equations. The stream function $\psi = \psi(x, y)$ use for this procedure is given as

125     $u = \frac{\partial \psi}{\partial y}, \ v = -\frac{\partial \psi}{\partial x},$ (7)

126   Where, equation (1) i.e. continuity equation is fulfilled identically. The similarity
127   transformations are characterized as

$$u = axf'(\eta), v = -\sqrt{av}f(\eta), \eta = y\sqrt{\frac{a}{v}}$$

128
$$\theta(\eta) = \frac{T-T_\infty}{T_w-T_\infty}, \phi(\eta) = \frac{C-C_\infty}{C_w-C_\infty}, \tag{8}$$

129

130 On substituting equation (8), system of equations (2) to (5) <u>is</u> converted to the following
131 nonlinear ordinary differential equations:

132

133 $(1+k)f''' + ff'' - f'^2 + kh' + (\lambda g + \delta q)cos\gamma - (M+K_1)f' = 0,$ $\hspace{2cm}$ (9)

134 $\left(1+\frac{k}{2}\right)h'' + fh' - f'h - k(2h+f'') = 0,$ $\hspace{3cm}$ (10)

135 $\left(\frac{1}{Pr}\right)\theta'' + f\theta' + Nb\phi'\theta' + Nt\theta'^2 = 0,$ $\hspace{3cm}$ (11)

136 $\phi'' + Lef\phi' + Nt_b\theta'' = 0,$ $\hspace{4cm}$ (12)

137

138 Where
139 $\lambda = \frac{Gr_x}{Re_x}, \delta = \frac{Gc_x}{Re_x}, M = \frac{\sigma B_0^2(x)}{a\rho}, K_1 = \frac{v}{ak}, Le = \frac{v}{D_B} Pr = \frac{v}{\alpha}, N_b = \frac{\tau D_B(C_w-C_\infty)}{v}, N_t = \frac{\tau D_t(T_w-T_\infty)}{vT_\infty},$
140 $Nt_b = \frac{N_t}{N_b}, Gr_x = \frac{g\beta_t(T_w-T_\infty)x}{av}, Re_x = \frac{u_w(x)x}{v}, Gc_x = \frac{g\beta_c(C_w-C_\infty)x}{av}$
141 (13)

142 Here, primes means the differentiation concerning η, λ Buoyancy constraint, Solutal buoyancy
143 parameter is given by δ, the magnetic parameter is given by M, kinematic viscidness of the
144 liquid is denoted by v, Pr denotes the Prandtl number, Le denotes the Lewis number, K_1
145 represents permeability factor, K is the dimensionless vertex thickness.

146

147 The corresponding boundary conditions are transformed to
148 $f(\eta) = 0, \quad f'(\eta) = 0, \theta(\eta) = 1, \phi(\eta) = 1 \quad at \ \eta = 0,$
149 $f'(\eta) \to 0, \quad \theta(\eta) \to 0, \phi(\eta) \to 0 \ as \ \eta \to \infty,$ $\hspace{2cm}$ (14)

150

151 The skin friction, Sherwood number and Nusselt number for the present problem are defined as

152

153 $Nu_x = \frac{xq_w}{k(T_w-T_\infty)}, Sh_x = \frac{xq_m}{D_B(C_w-C_\infty)}, C_f = \frac{t_w}{u_w^2\rho_f}$ $\hspace{2cm}$ (15)

154 The related terms for the skin-friction factor $C_{fx}(0) = f''(0)$, the reduced Nusselt number $-\theta'(0)$

155 and the reduced Sherwood number $-\phi'(0)$ are defined as

156 $-\theta'(0) = \frac{Nu_x}{\sqrt{Re_x}}, -\phi'(0) = \frac{Sh_x}{\sqrt{Re_x}}, C_{fx} = C_f\sqrt{Re_x}$ $\hspace{2cm}$ (16)

157 Where, $Re_x = \frac{u_w(x)x}{v}$, is the local Reynolds number built on the extending velocity. The
158 converted nonlinear differential equations (9) to (12) by applying equation (14) are elucidated by

159 Keller box scheme consisting on the steps as, finite-differences technique, Newton's scheme and
160 block elimination process clearly explained by Anwar et al. [30].

161

162 **3 Results and Discussion**

163 This portion of study deals with the calculated results of converted nonlinear ordinary
164 differential equations (9-12) with boundary conditions (14) solved via Killer-box method. For
165 numerical result of physical parameters of our concern including Brownian motion
166 constraint Nb, thermophoresis constraint Nt, magnetic factor M, buoyancy factor λ, solutal
167 buoyancy factor δ, inclination factor γ, Prandtl number Pr, Lewis number Le, and material
168 factor K several figures and tables are prepared. In Table 3.1, in the deficiency of buoyancy
169 factor λ, solutal buoyancy factor δ, magnetic factor M, porosity parameter K_1 and material
170 parameter K with $\gamma = 90^o$ outcomes for reduced Nusselt number $-\theta'(0)$, reduced Sherwood
171 number $-\phi'(0)$ are equated with the existing results of Khan and Pop [31]. The consequences
172 are established brilliant settlement. The effects of reduced Nusselt number $-\theta'(0)$, reduced
173 Sherwood number $-\phi'(0)$ and skin friction coefficient $C_{fx}(0)$ against altered values of involved
174 physical parameters $Nb, Nt, M, K, \lambda, \delta, \gamma, K_1, Le$, and Pr are shown in table 3.2. It is eminent
175 that $-\theta'(0)$ declines for increasing the values of $Nb, Nt, M, Le, K_1, \gamma$, and increased by enhancing
176 the numerical values of K, λ, δ, and Pr. Moreover, it is perceived that $-\phi'(0)$ enhanced with the
177 larger values of $Nb, \lambda, \delta, Nt, Le, K$ and drops for bigger values of M, K_1, Pr and γ. On the other
178 hand, $C_{fx}(0)$ rises with the growing values of $Nb, Le, M, K, \gamma, K_1$, and drops with the higher
179 values of Nt, λ, δ, and Pr.

180

181

182

183

184

185

186

187

188

189

190 **Table 3.1:** Contrast of the reduced Nusselt number $-\theta'(0)$ and the reduced Sherwood number

191 $-\phi'(0)$ when M, K, K1, δ , λ $= 0$, $\Pr = Le = 10$ and $\gamma = 90^{\circ}$.

192

Nb	*Nt*	Khan and Pop (2010)		Present Results	
		$-\theta'(0)$	$-\phi'(0)$	$-\theta'(0)$	$-\phi'(0)$
0.1	0.1	0.9524	2.1294	0.9524	2.1294
0.2	0.2	0.3654	2.5152	0.3654	2.5152
0.3	0.3	0.1355	2.6088	0.1355	2.6088
0.4	0.4	0.0495	2.6038	0.0495	2.6038
0.5	0.5	0.0179	2.5731	0.0179	2.5731

193

194

195

196

197

198

199

200

201

202

203

204

205 **Table 3.2:** Values of the reduced Nusselt number $-\theta'(0)$, the reduced Sherwood number
206 $-\phi'(0)$ and the Skin-friction coefficient $C_{fx}(0)$.

Nb	*Nt*	**Pr**	*Le*	*M*	*K*	*λ*	*δ*	*K1*	*γ*	$-\theta'(0)$	$-\phi'(0)$	$C_{fx}(0)$
0.1	0.1	7.0	5.0	0.5	1.0	0.1	0.9	1.0	45^0	1.1054	1.0880	1.8913
0.5	0.1	7.0	5.0	0.5	1.0	0.1	0.9	1.0	45^0	0.2060	1.6011	1.9459
0.1	**0.5**	7.0	5.0	0.5	1.0	0.1	0.9	1.0	45^0	0.5104	1.3906	1.7176
0.1	0.1	**10.0**	5.0	0.5	1.0	0.1	0.9	1.0	45^0	1.1531	1.0852	1.8882
0.1	0.1	7.0	**10.0**	0.5	1.0	0.1	0.9	1.0	45^0	0.9672	2.0567	1.9689
0.1	0.1	7.0	5.0	**1.0**	1.0	0.1	0.9	1.0	45^0	1.0949	1.0550	2.1075
0.1	0.1	7.0	5.0	0.5	**3.0**	0.1	0.9	1.0	45^0	1.1331	1.1755	2.6215
0.1	0.1	7.0	5.0	0.5	1.0	**0.5**	0.9	1.0	45^0	1.1090	1.0963	1.8040
0.1	0.1	7.0	5.0	0.5	1.0	0.1	**2.0**	1.0	45^0	1.1195	1.1254	1.5847
0.1	0.1	7.0	5.0	0.5	1.0	0.1	0.9	**2.0**	45^0	1.0851	1.0246	2.3071
0.1	0.1	7.0	5.0	0.5	1.0	0.1	0.9	1.0	**90^0**	1.0917	1.0507	2.1758

207
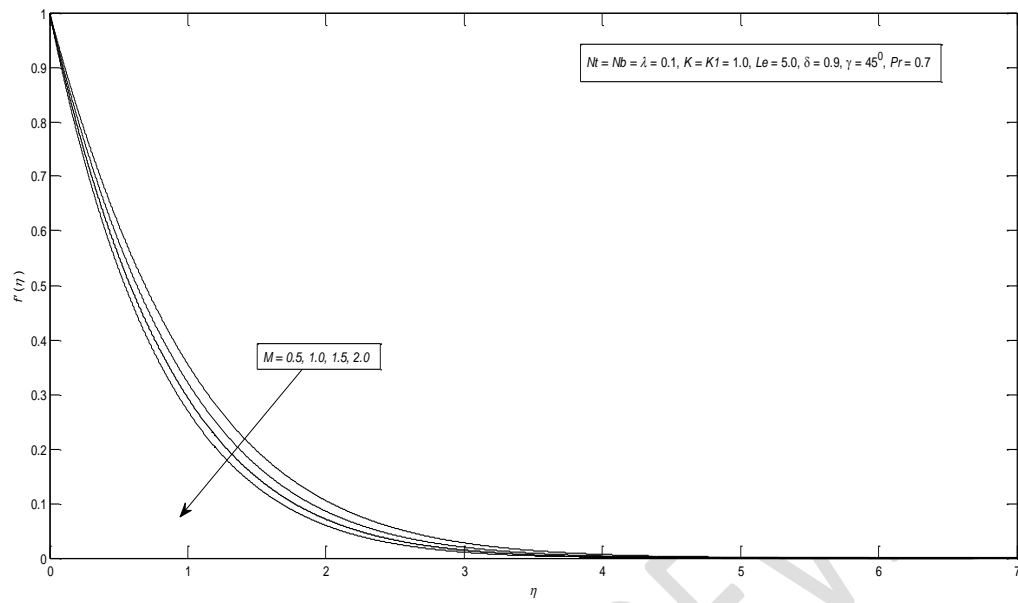
208

209   Fig. 2. Variations in velocity profile for several values of M.
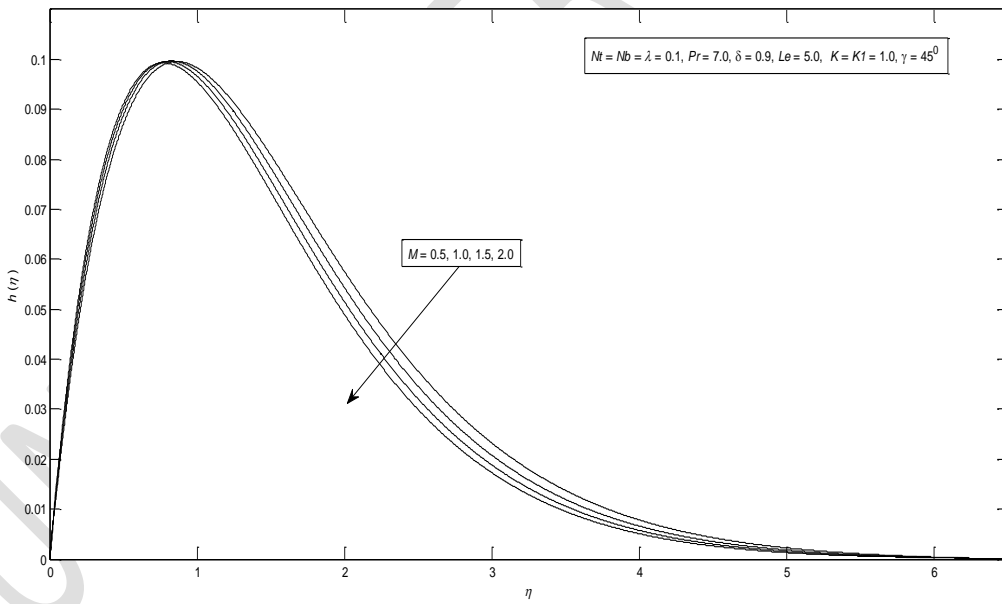
210

211   Fig. 3. Variations in angular velocity for several values of M.

212
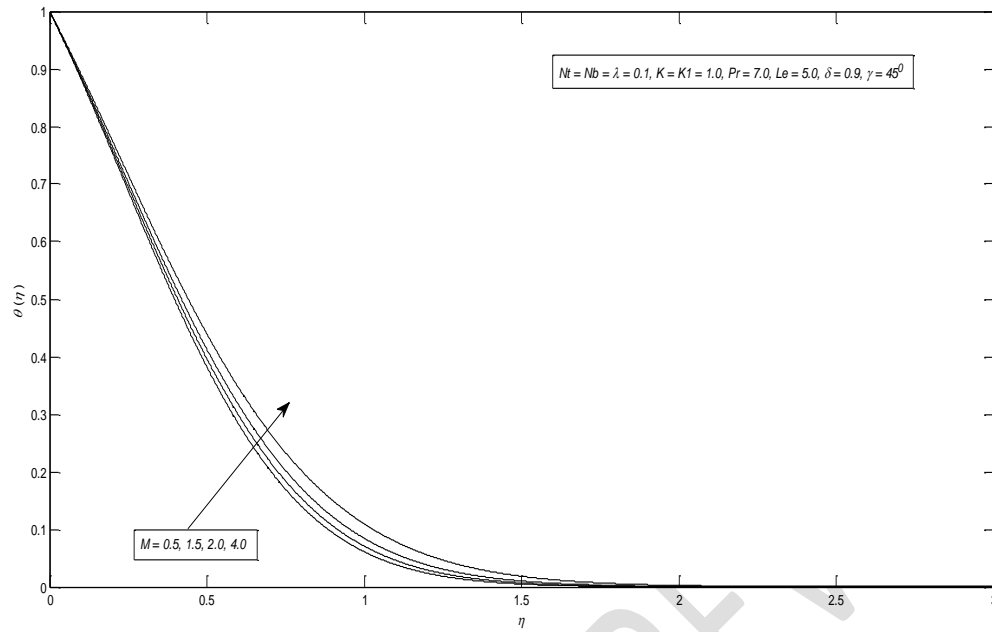
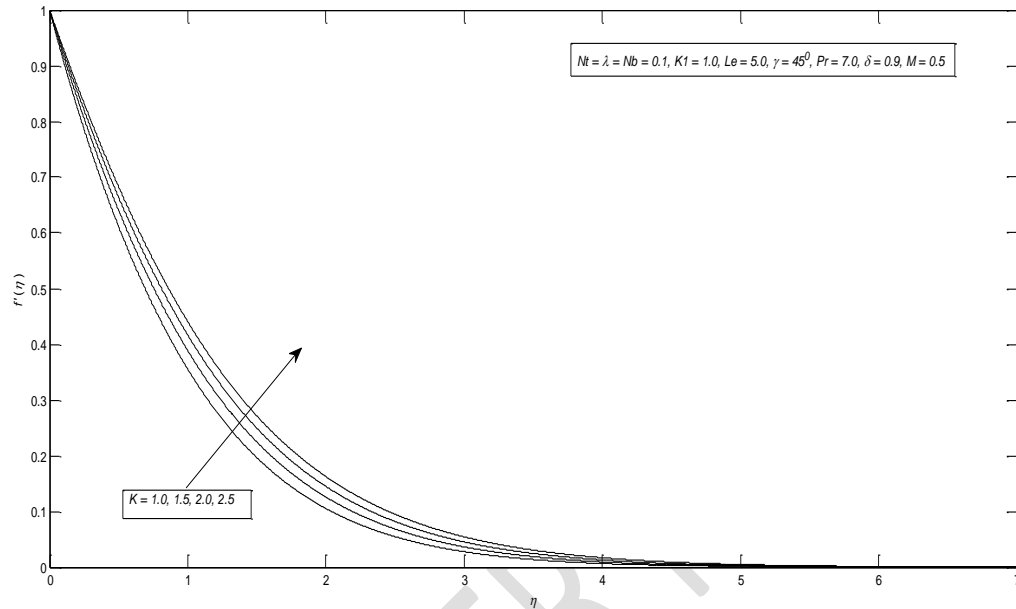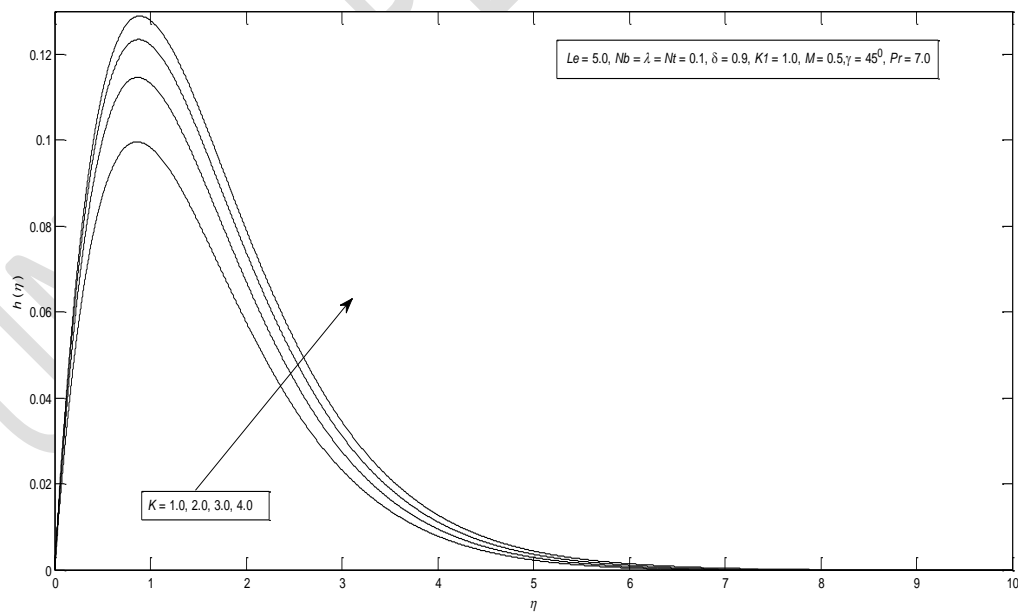Fig. 4. Variations in temperature profile for several values of M.

214
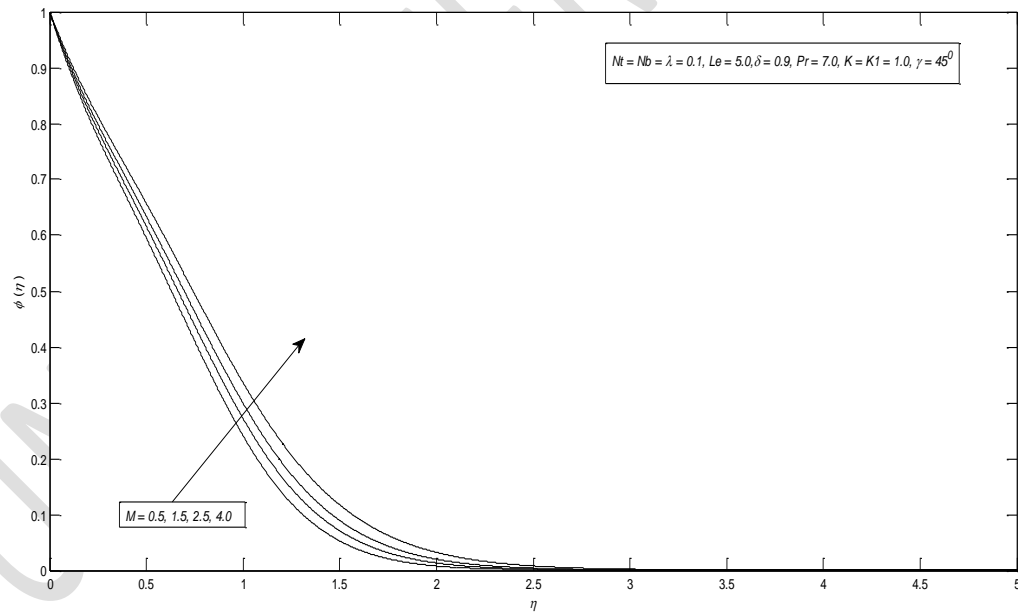
Fig. 5. Variations in concentration profile for several values of M.

Fig. 2 gives a picture of the upshot of factor M on velocity profile. The velocity outline slows
down as we upsurge the magnetic field constraint M. It is seensince the use of magnetic field
yields Lorentz force, by means retard the speed of the fluid. The similar result has seen in the

219   instance of the angular velocity against changed values of M in Fig. 3. Whereas, the different
220   impacts of M on the temperature distribution <u>are</u> presented in Fig. 4 and concentration profile in
221   Fig. 5.

222

Fig. 6. Variations in velocity profile for several values of K.

224

Fig. 7. Variations in angular velocity profile for several values of K.
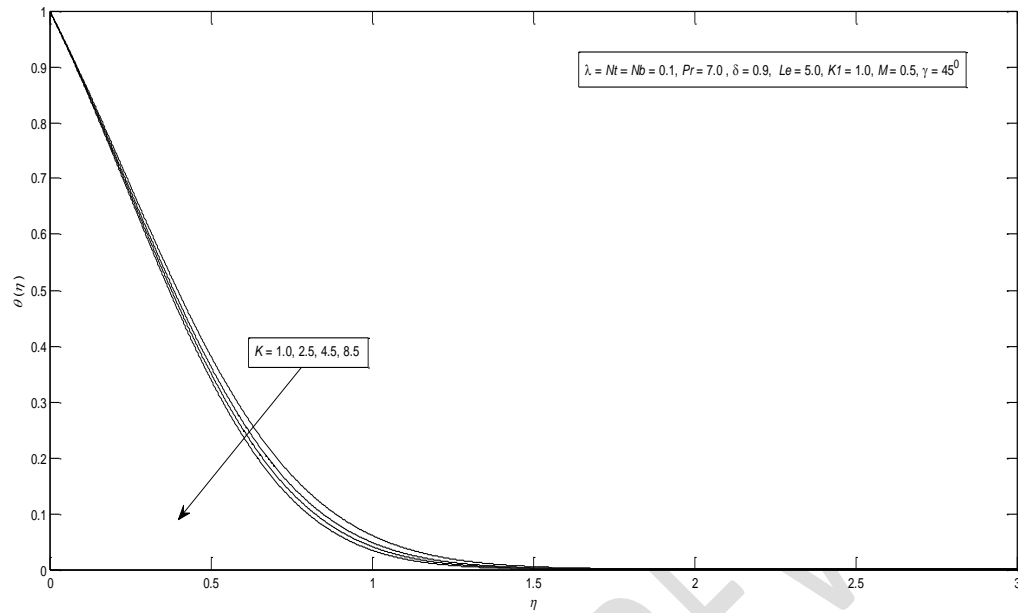
226

227 Fig. 8. Variations in temperature profile for several values of K.
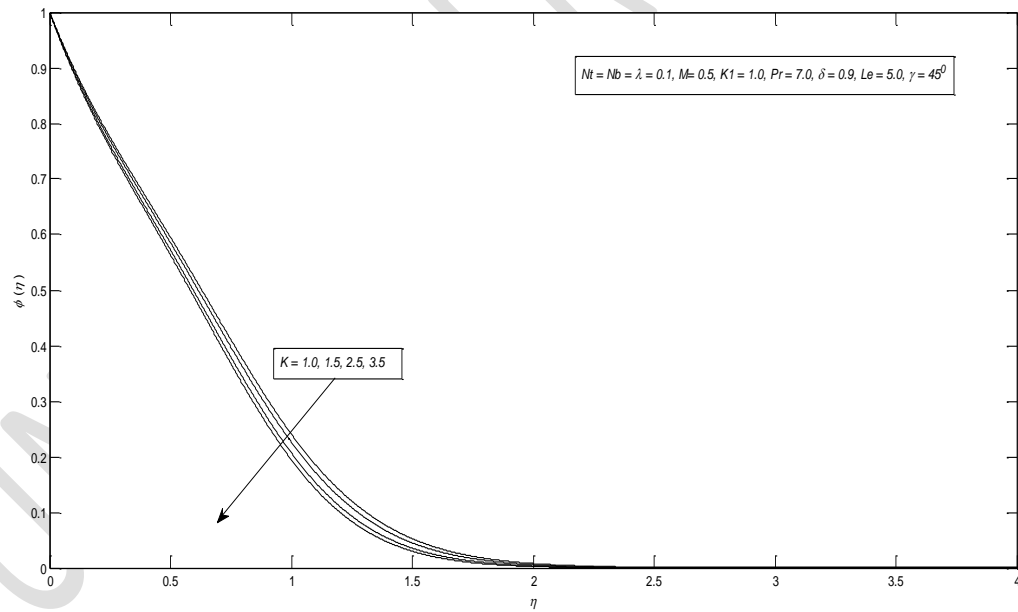
228

229 Fig. 9. Variations in concentration profile for several values of K.

230 It is noticed in Fig.6 the velocity profile upturn by enhancing the values of K. The angular
231 velocity profile rise by growing the values of K is indicateds in Fig. 7. The boundary layer
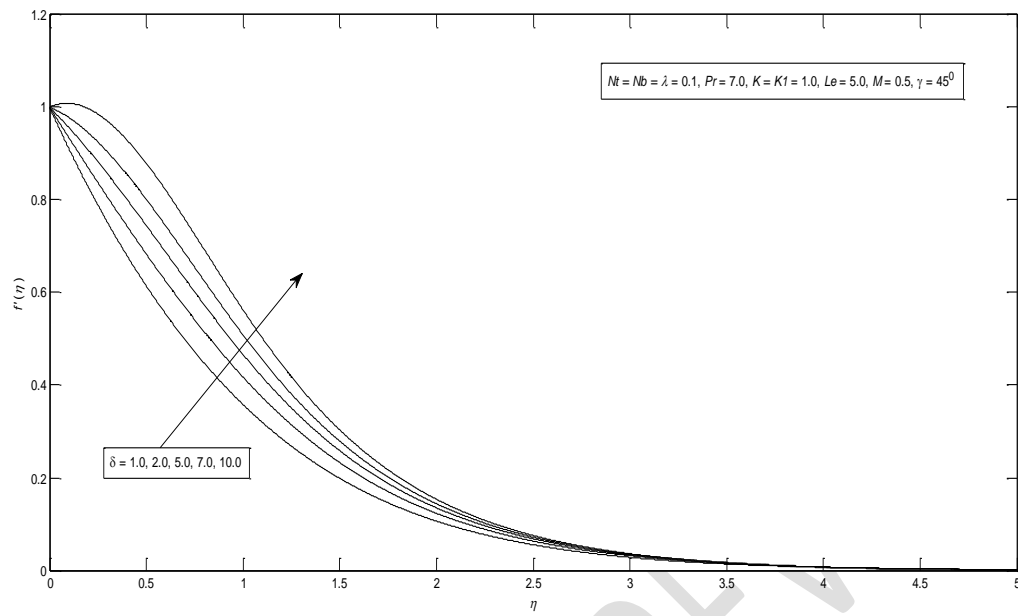
232 thickness losses by improving the values of K. On the other hand, Figs. 8 and 9 depict the
233 opposite effects against different values of K.
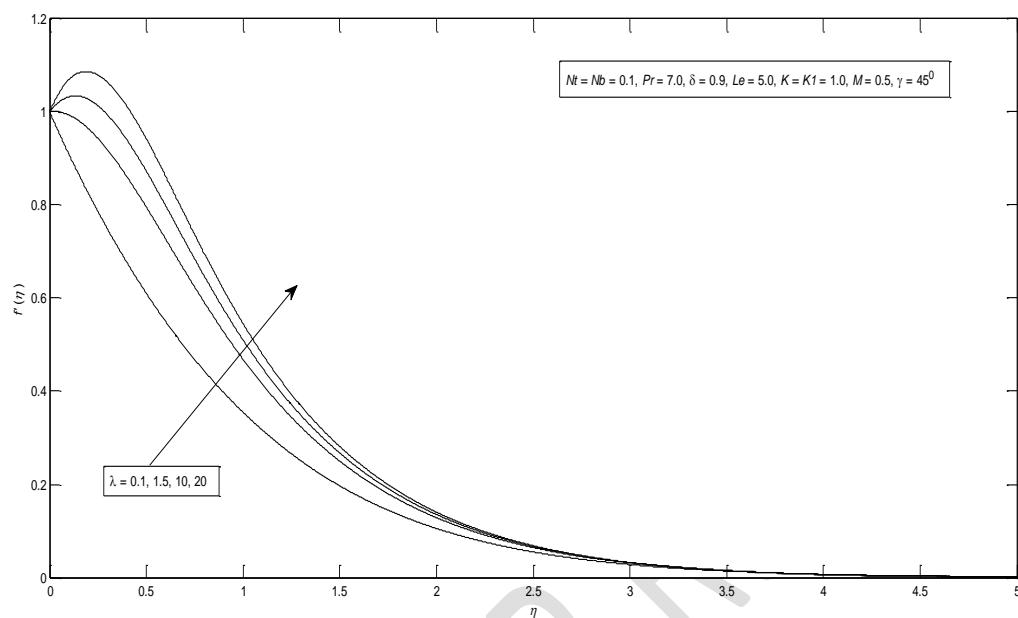
234

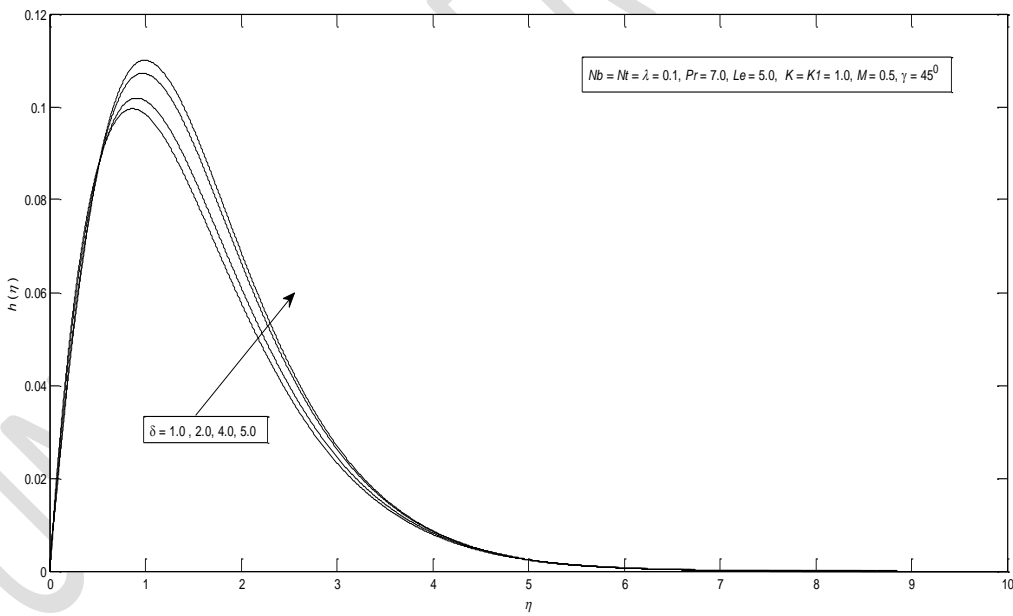235 Fig. 10. Variations in velocity profile for several values of λ.
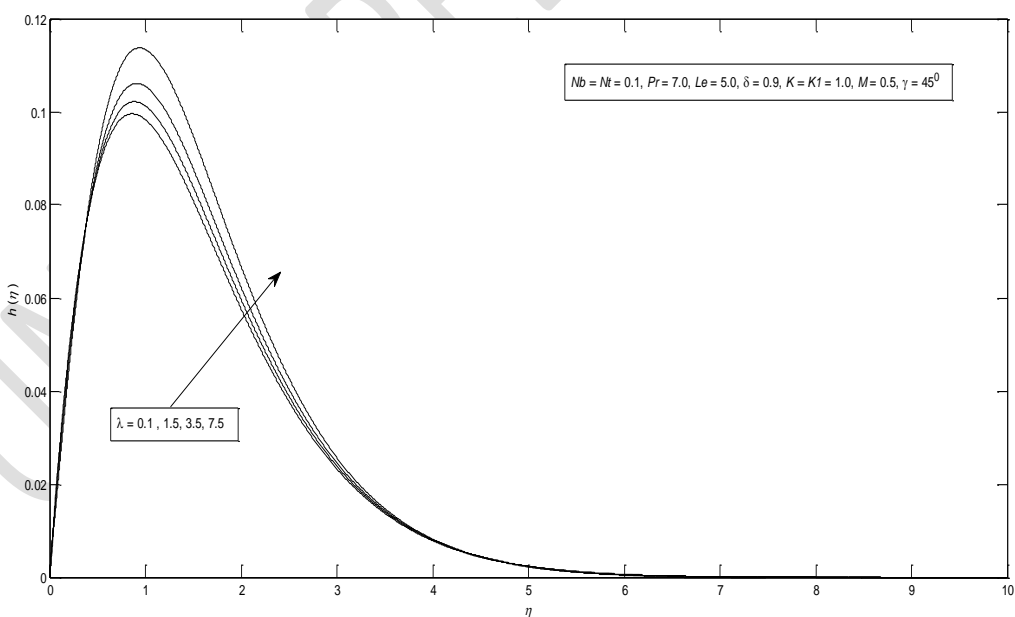
236

237 Fig. 11. Variation in angular velocity profile for sevral values of λ.

238

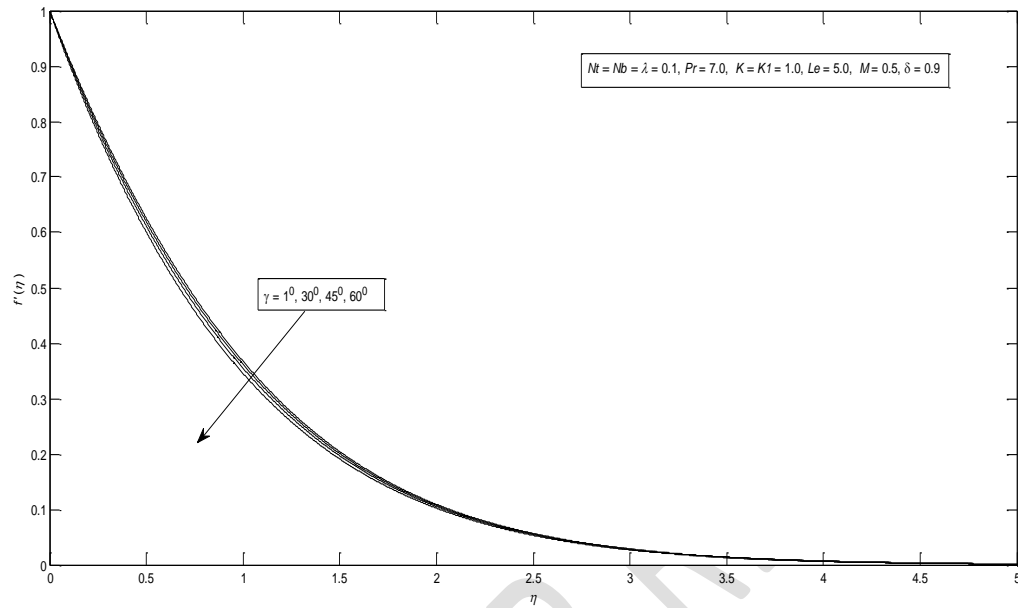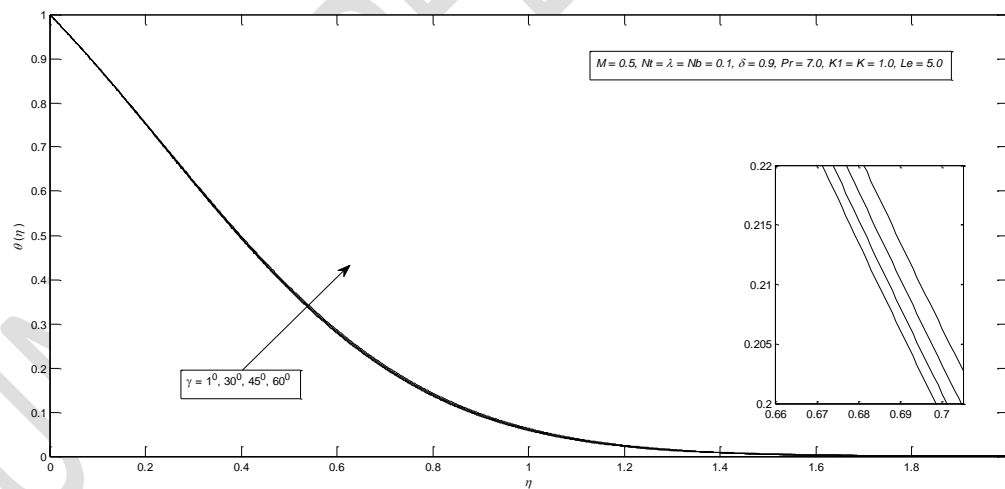Fig. 12. Variations in velocity profile for several values of δ.

240

Fig. 13. Variations in angular velocity profile for several values of δ.

The velocity shape upturns in Fig. 10 by enhancing bouncy parameter λ. Similarly the angular velocity also enhanced with large values of λ clearly shown in Fig. 11. Moreover, the similar

244 | result for solutal bouncy parameter δ on velocity distribution and angular velocity contour is
245 | prominent in Figs.12 and 13.

246

247   Fig. 14. Variations in velocity profile for several value of γ.

248

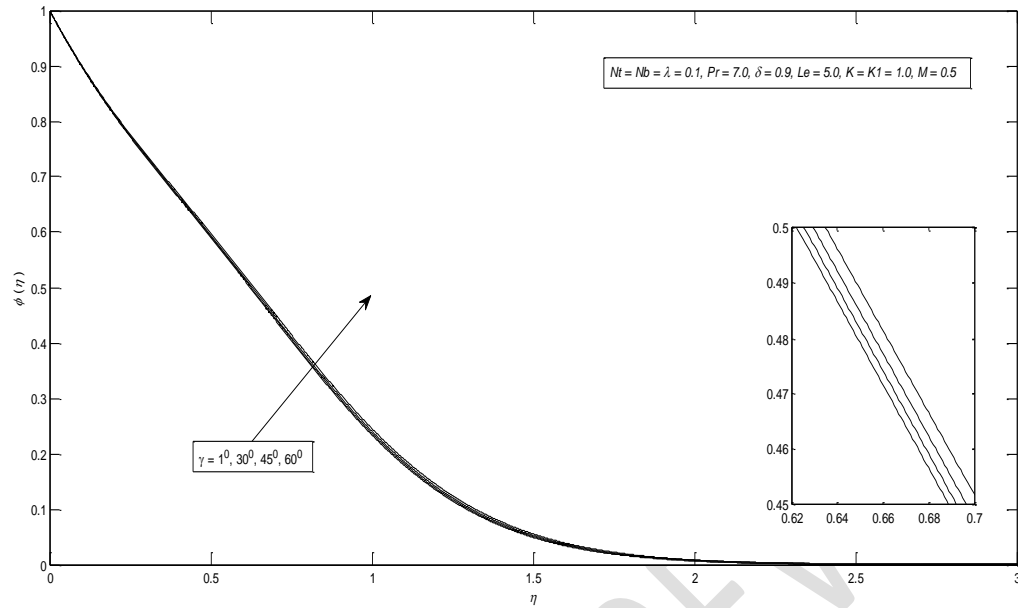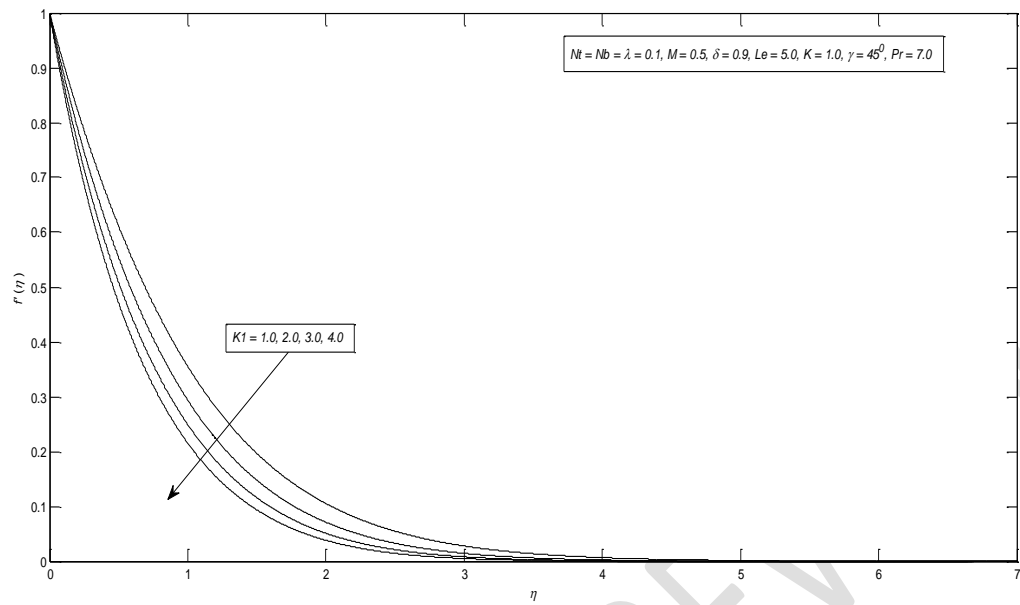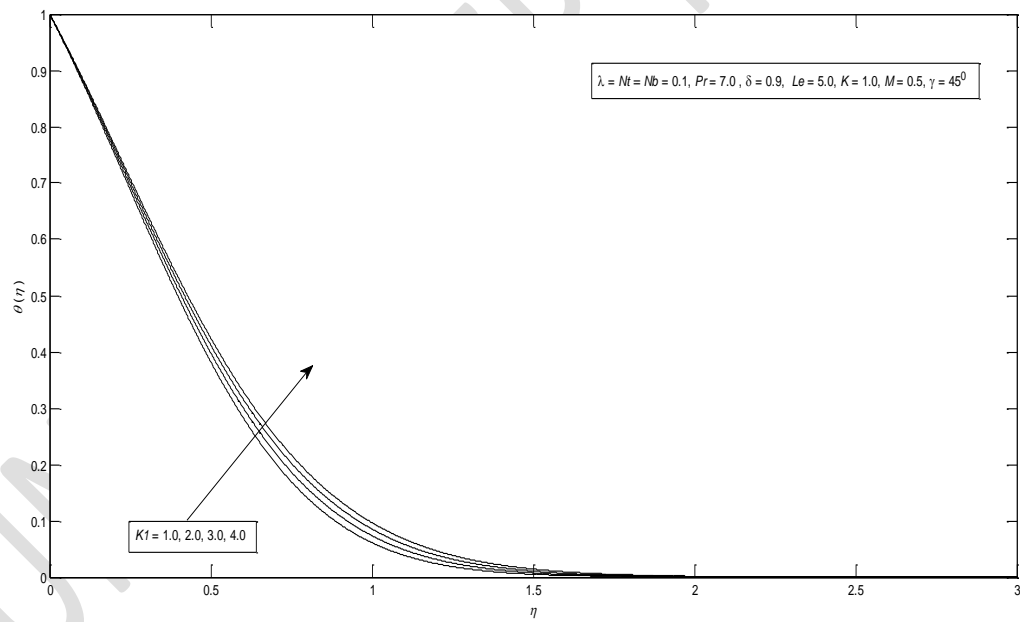249   Fig. 15. Variations in temperature profile for several values of γ.

250

Fig. 16. Variations in concentration profile for several values of γ.

Fig. 14 portrays the consequence of inclination factor γ on velocity outline. It is openly perceived the velocity outline depreciate as we enhance the values of inclination parameter γ. This can be ascribed to the circumstance that the maximum gravitational force act on flow when the inclination parameter $\gamma = 0$ because in this situation the sheet will be vertical. On the other hand, for $\gamma = 90^0$ the sheet will be horizontal which cause the reduction in the velocity profile as the strength of the bouncy forces decrease. Besides, opposite result are recovered in Figs. 15 and 16 for large values of inclination parameter γ in the instance of temperature and concentration sketches.

Fig. 17. Variations in velocity profile for several values of K_1.

Fig. 18. Variations in temperature profile for several value of K_1.

The chart contains the annotation: $Nt = Nb = \lambda = 0.1$, $M = 0.5$, $K = 1.0$, $Pr = 7.0$, $\delta = 0.9$, $Le = 5.0$, $\gamma = 45^0$

The y-axis is labeled $\phi(\eta)$ and the x-axis is labeled η.

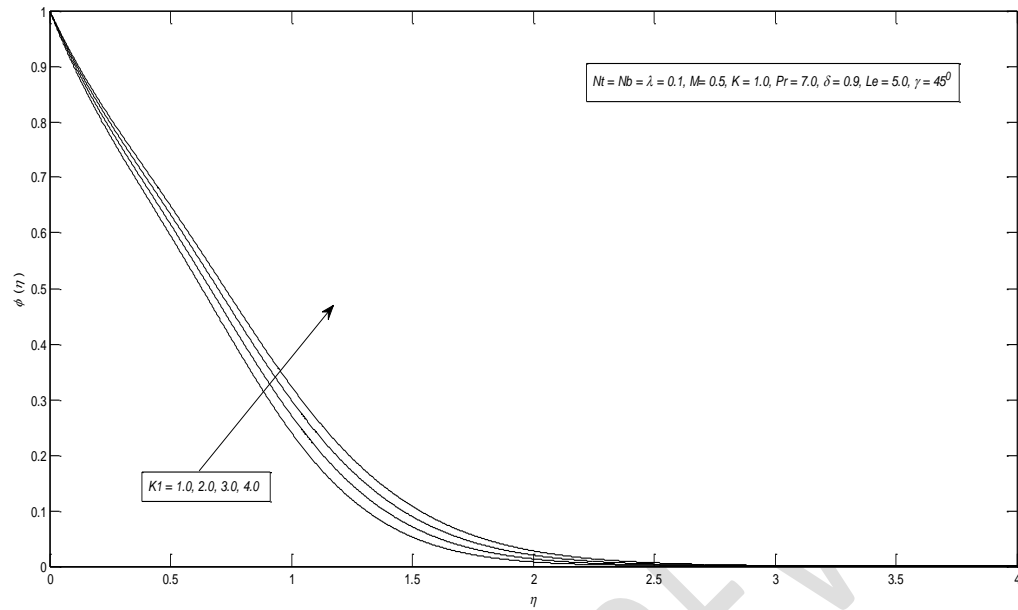An inner label reads: $K1 = 1.0, 2.0, 3.0, 4.0$

264

265   Fig. 19. Variations in concentration profile for several values of K_1.

266   It is well known that the porous medium offers high resistance that cause rising of shear stress.
267   This shear stress work opposite to the fluid motion over a stretching sheet and fluid motion tends
268   to slow. That's why, velocity profile illustrate reduction by increasing the values of K_1 in this
269   case as indicated by Fig. 17. Moreover, oppoite impact is ilustrated in Figs. 18 and 19 for
270   vaerious values of K_1.
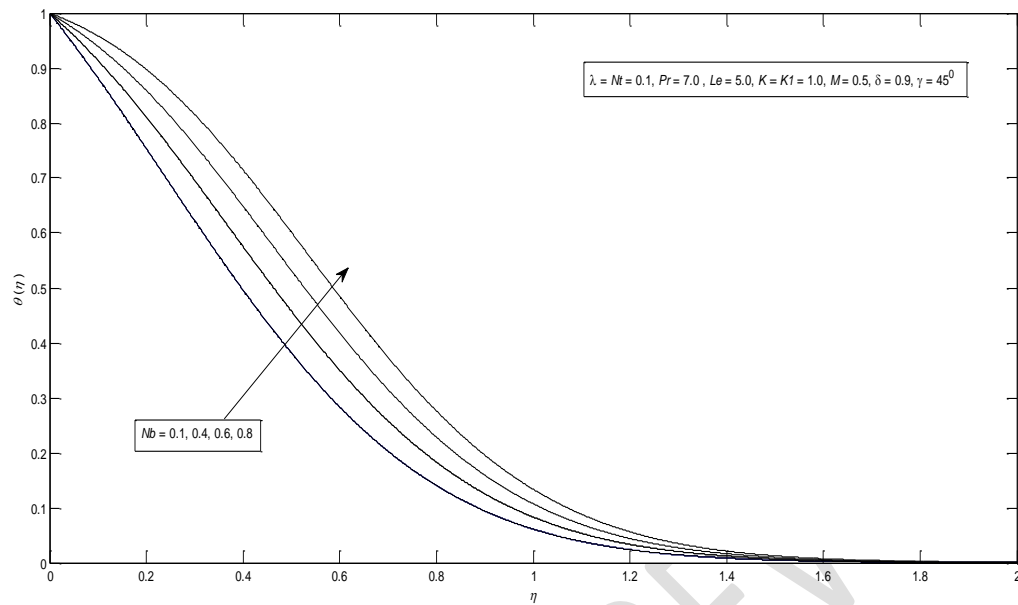
271
272 Fig. 20. Variations in temperature profile for several values of Nb.
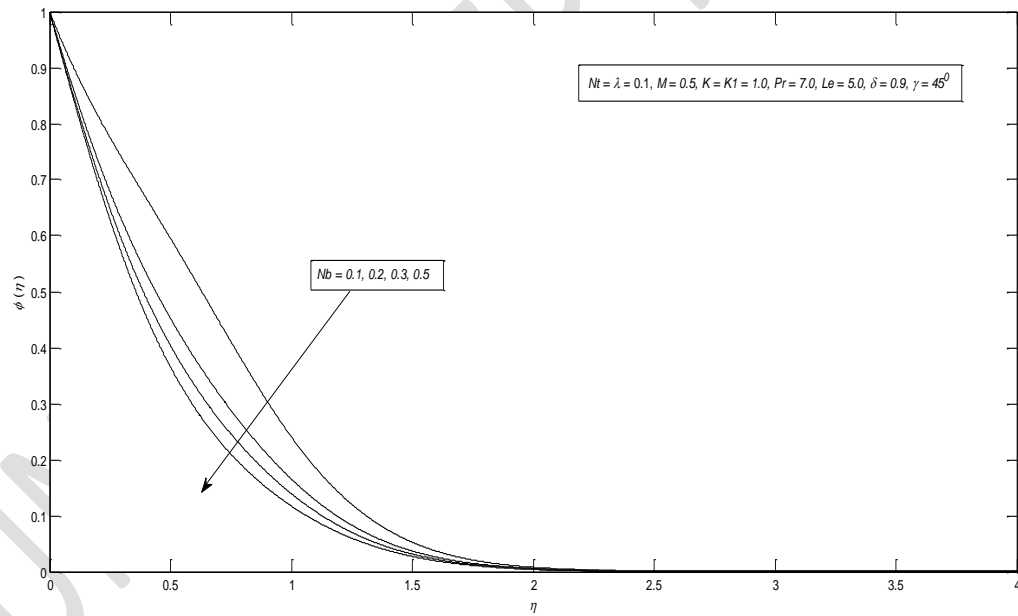

273

274 Fig. 21. Variations in concentration profile for several values of Nb.

275 Figures. 20 and 21 display the of effect of Brownian movement on the temperature and
276 concentration sketches separately. The temperature sketch enlarges on enlarging Nb, on the other
277 hand, concentration distribution enlighten dissimilar style. Physically, boundary layer heat up

278   due to the development in Brownian motion which inclines to travel nanoparticles from the
279   extending sheet to the motionless liquid. Therefore the absorption nanoparticle lessens.
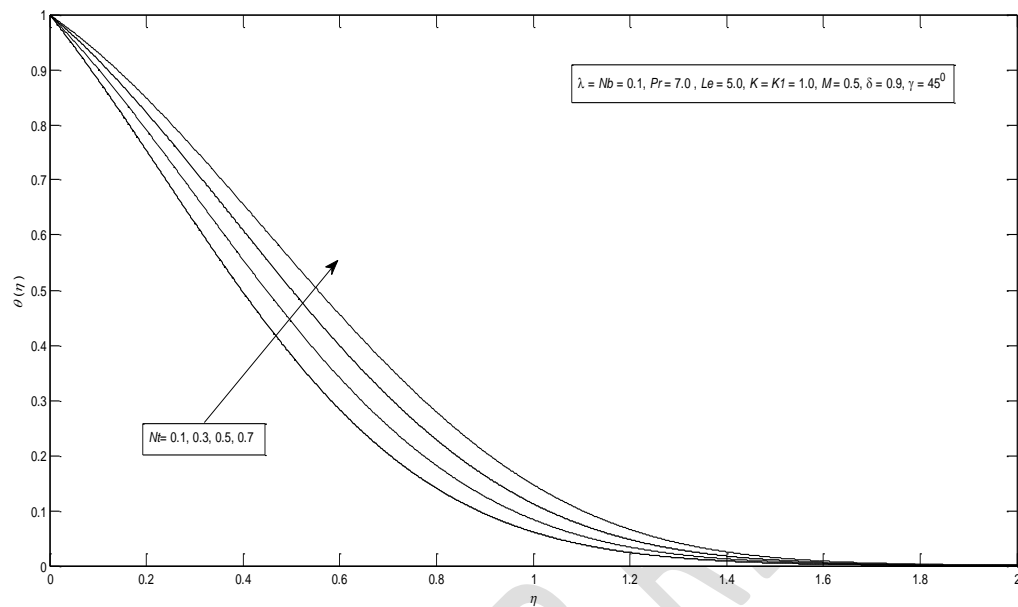
280

281   Fig. 22. Variations in temperature profile for several values of Nt.
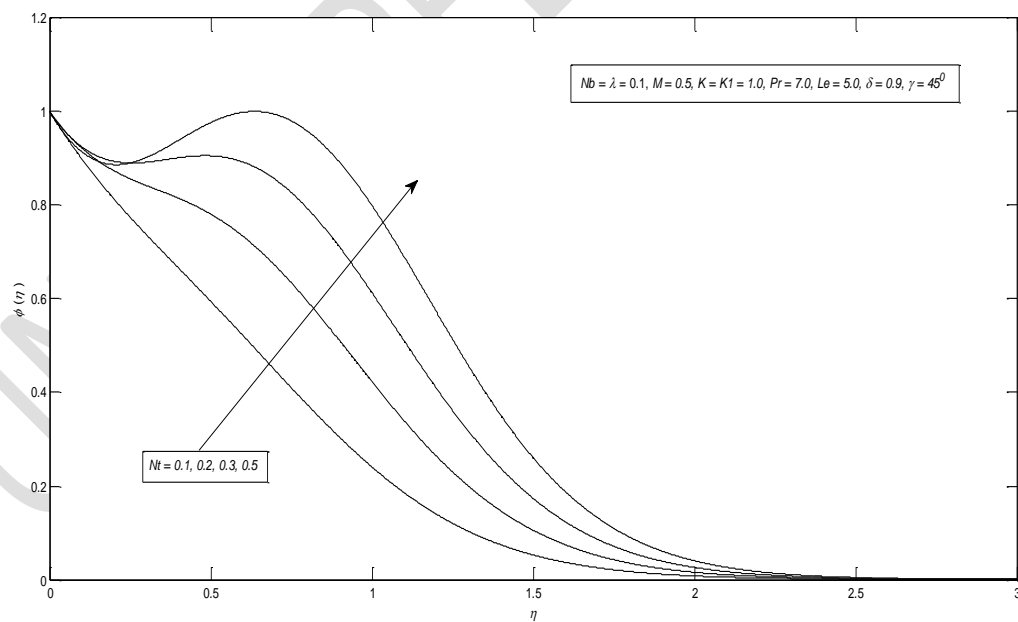
282

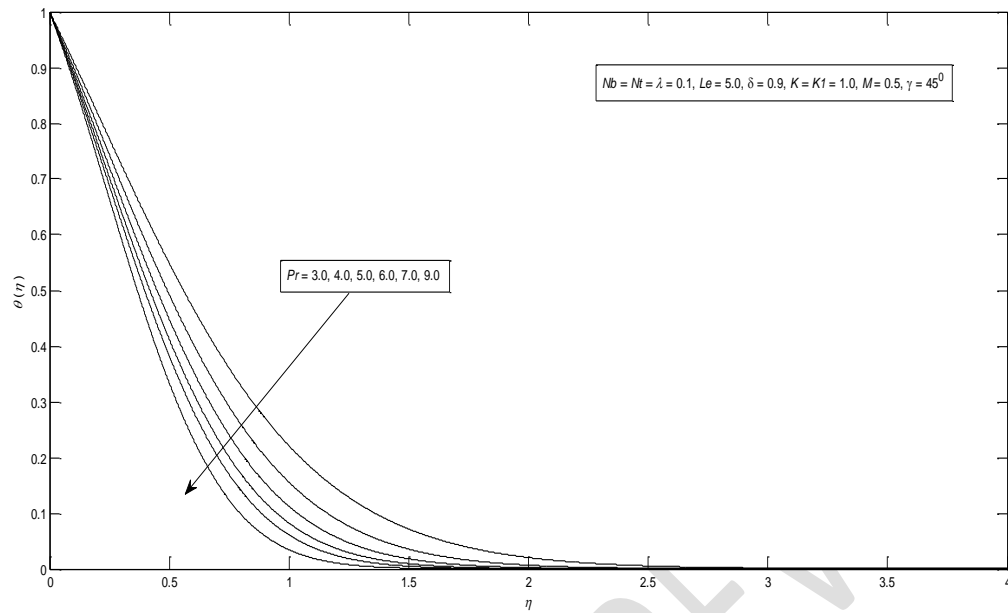283   Fig. 23. Variations in concentration profile for several values of Nt.

284
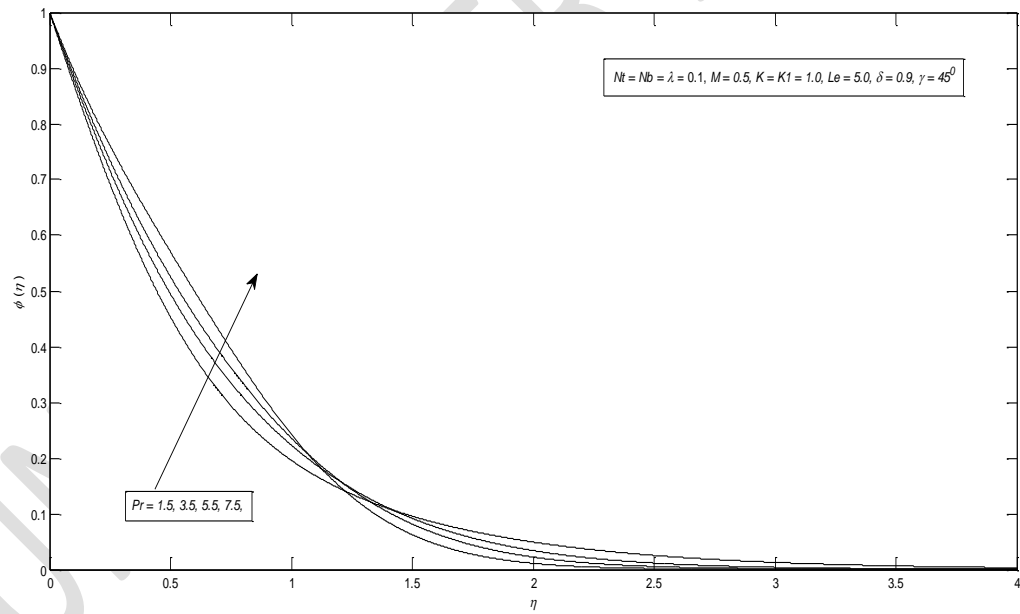285   Fig. 24. Variations in temperature profile for several values of Pr.

286

287   Fig. 25. Variations in concentration profile for several values of Pr.

The plot legend reads: $Nb = Nt = \lambda = 0.1,\ M = 0.5,\ Pr = 7.0,\ K = K1 = 1.0,\ \delta = 0.9,\ \gamma = 45^0$
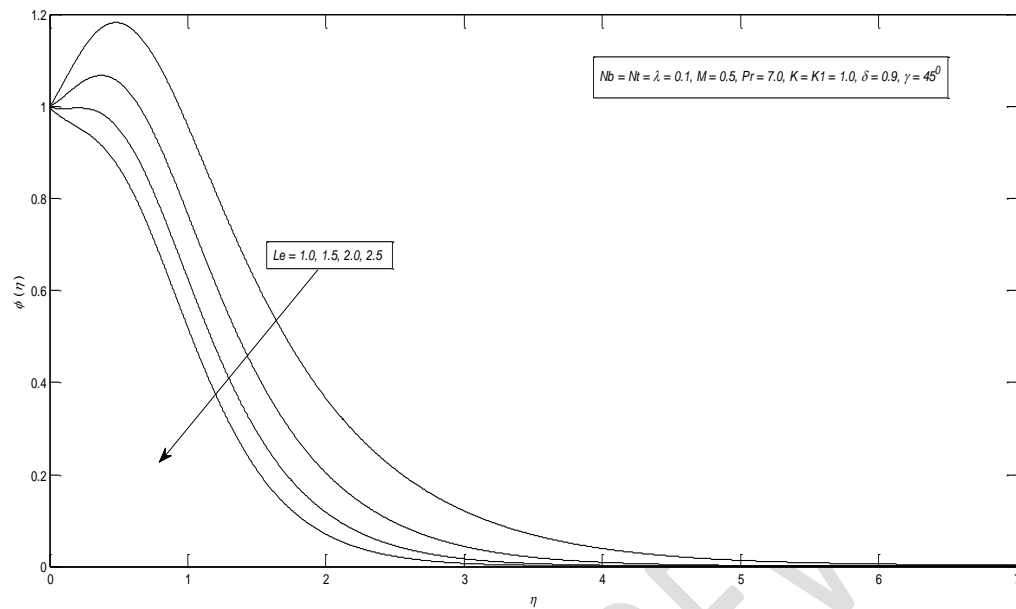
$Le = 1.0,\ 1.5,\ 2.0,\ 2.5$

288

289   Fig. 26. Variations in concentration profile for several value of Le.

290   Figs. 22 and 23 present temperature and concentration profile against several values of
291   thermophoresis parameters Nt. It is observed that both temperature and concentration contours
292   upsurge by growing the thermophoresis parameter. Thermophoresis works to heat up boundary
293   layer against several values of Prandtl number and Lewis number. Besides the amount of heat
294   and mass exchange reduce by improving thermophoresis constraint Nt. Fig. 24 reveals that by
295   growing the values of Prandtl number factor Pr the temperature profile drop, because thermal
296   boundary layer viscosity declining by growing the Prandtl number Pr. In short, an upturn in
297   Prandtl number Pr mean deliberate amount of thermal dispersion. Whereas, concentration
298   profile fall with large values of Pr presented in Fig. 25. Fig. 26 displays the result of Lewis
299   number Le on concentration profile. The boundary layer viscosity lessening by improving the
300   values of Lewis number Le.

4 Conclusions

302   This study is has explored the heat and mass exchange of micropolar nanofluid flow over linear
303   inclined extending sheet. It is noted that $-\theta'(0)$ falls for growing the values of Nb, Nt, M, Le, K_1,
304   γ, and improved by enhancing the numerical values of K, λ, δ, and Pr. Moreover, it is observed
305   that $-\phi'(0)$ boosted with the larger values of $Nb, \lambda, \delta, Nt, Le, K$ and falls for bigger values of
306    $M, K_1,\ Pr$ and γ. On the other hand, $C_{fx}(0)$ rises with the cumulative values of Nb, Le, M, K, γ,
307   K_1, and falls with the higher values of Nt, λ, δ, and Pr.

308

309

310

References

[1] Choi, S. U. S., Singer, D. A., & Wang, H. P. (1995). Developments and applications of non-Newtonian flows. *ASME FED*, *66*, 99–105.

[2] Buongiorno, J. (2006). Convective transport in nanofluids. *Journal of Heat Transfer*, *128*(3), 240–250.

[3] Zaimi, K., Ishak, A., & Pop, I. (2014). Boundary layer flow and heat transfer over a nonlinearly permeable stretching/shrinking sheet in a nanofluid. *Scientific Reports*, *4*, 4404.

[4] Anwar, M. I., Khan, I., Sharidan, S., & Salleh, M. Z. (2012). Conjugate effects of heat and mass transfer of nanofluids over a nonlinear stretching sheet. *International Journal of Physical Sciences*, *7*(26), 4081-4092.

[5] Sandeep, N., & Kumar, M. S. (2016). Heat and Mass Transfer in Nanofluid Flow over an Inclined Stretching Sheet with Volume Fraction of Dust and Nanoparticles. *Journal of Applied Fluid Mechanics*, *9*(5).

[6] Suriyakumar, P., & Devi, S. A. (2015). Effects of Suction and Internal Heat Generation on Hydromagnetic Mixed Convective Nanofluid Flow over an Inclined Stretching Plate. *European journal of advances in engineering and technology*, *2*(3), 51-58.

[7] Ziaei-Rad, M., Kasaeipoor, A., Rashidi, M. M., & Lorenzini, G. (2017). A Similarity Solution for Mixed-Convection Boundary Layer Nanofluid Flow on an Inclined Permeable Surface. *Journal of Thermal Science and Engineering Applications*, (c). https://doi.org/10.1115/1.4035733

[8] Rashad, A. (2017). Unsteady nanofluid flow over an inclined stretching surface with convective boundary condition and anisotropic slip impact. *International Journal of Heat and Technology*, *35*(1), 82–90. https://doi.org/10.18280/ijht.350111

[9] Mitra, A. (2018). Computational Modelling of Boundary-Layer Flow of a Nano fluid Over a Convective Heated Inclined Plate. *JOURNAL OF MECHANICS OF CONTINUA AND MATHEMATICAL SCIENCES*, *13*(2), 88-94.

[10] Khan, M., Shahid, A., Malik, M. Y., & Salahuddin, T. (2018). Thermal and concentration diffusion in Jeffery nanofluid flow over an inclined stretching sheet: A generalized Fourier's and Fick's perspective. *Journal of Molecular Liquids*, *251*, 7–14.

[11] Hatami, M., Jing, D., & Yousif, M. A. (2018). Three-dimensional analysis of condensation nanofluid film on an inclined rotating disk by efficient analytical methods. *Arab Journal of Basic and Applied Sciences*, *25*(1), 28–37.

[12] Sakiadis, B. C. (1961). Boundary-layer behavior on continuous solid surfaces: I. Boundary-layer equations for two-dimensional and axisymmetric flow. *AIChE Journal*, *7*(1), 26–28.

345

[13] Crane, L. J. (1970). Flow past a stretching plate. *Zeitschrift Für Angewandte Mathematik Und Physik (ZAMP)*, *21*(4), 645–647.

[14] Ramesh, G. K., Gireesha, B. J., & Bagewadi, C. S. (2012). Heat transfer in MHD dusty boundary layer flow over an inclined stretching sheet with non-uniform heat source/sink. *Advances in Mathematical Physics*, *2012*.

[15] Singh, P. K. (2012). Heat and mass transfer in MHD boundary layer flow past an inclined plate with viscous dissipation in porous medium. *International Journal of Scientific & Engineering Research*, *3*(6), 1–11.

[16] Ali, M., Alim, M. A., & Alam, M. S. (2015). Similarity Solution of Heat and Mass Transfer Flow over an Inclined Stretching Sheet with Viscous Dissipation and Constant Heat Flux in Presence of Magnetic Field. *Procedia Engineering*, *105*(Icte 2014), 557–569. https://doi.org/10.1016/j.proeng.2015.05.089

[17] Ramesh, G. K., Chamkha, A. J., & Gireesha, B. J. (2015). Boundary layer flow past an inclined stationary/moving flat plate with convective boundary condition. *Afrika Matematika*. https://doi.org/10.1007/s13370-015-0323-x

[18] Malik, M. Y., & Rehman, K. U. (2016). Effects of second order chemical reaction on MHD free convection dissipative fluid flow past an inclined porous surface by way of heat generation: A Lie group analysis. *Information Sciences Letters*, *5*, 35-45.

[19] Hayat, T., Qayyum, S., Alsaedi, A., & Asghar, S. (2017). Radiation effects on the mixed convection flow induced by an inclined stretching cylinder with non-uniform heat source/sink. *PloS one*, *12*(4), e0175584.

[20] Balla, C. S., Kishan, N., Gorla, R. S. R., & Gireesha, B. J. (2017). MHD boundary layer flow and heat transfer in an inclined porous square cavity filled with nanofluids. *Ain Shams Engineering Journal*, *8*(2), 237–254.

[21] Eringen, A. C. (1964). Simple microfluids. *International Journal of Engineering Science*, *2*(2), 205–217.

[22] Rahman, M. M., Aziz, A., & Al-Lawatia, M. A. (2010). Heat transfer in micropolar fluid along an inclined permeable plate with variable fluid properties. *International Journal of Thermal Sciences*, *49*(6), 993–1002. https://doi.org/10.1016/j.ijthermalsci.2010.01.002

[23] Das, K. (2012). Slip effects on heat and mass transfer in MHD micropolar fluid flow over an inclined plate with thermal radiation and chemical reaction. *International Journal for Numerical Methods in Fluids*, *70*(1), 96–113.

[24] Kasim, A. R. M., Mohammad, N. F., & Shafie, S. (2013). Unsteady MHD mixed convection flow of a micropolar fluid along an inclined stretching plate. *Heat Transfer—Asian Research*, *42*(2), 89–99.

[25] Srinivasacharya, D., & Bindu, K. H. (2016). Entropy generation in a micropolar fluid flow

382   through an inclined channel. *Alexandria Engineering Journal*, *55*(2), 973–982.

383 [26] Hazbavi, A., & Sharhani, S. (2017). Micropolar Fluid Flow Between Two Inclined Parallel
384   Plates. In *ASME 2017 International Mechanical Engineering Congress and Exposition* (p.
385   V008T10A085-V008T10A085). American Society of Mechanical Engineers.

386 [27] Shamshuddin, M. D., Mishra, S. R., Bég, O. A., & Kadir, A. (2018). Unsteady reactive
387   magnetic radiative micropolar flow, heat and mass transfer from an inclined plate with joule
388   heating: A model for magnetic polymer processing. *Proceedings of the Institution of*
389   *Mechanical Engineers, Part C: Journal of Mechanical Engineering Science*,
390   954406218768837.

391 [28] Srinivasacharya, D., RamReddy, C., & Naveen, P. (2018). Double dispersion effect on
392   nonlinear convective flow over an inclined plate in a micropolar fluid saturated non-Darcy
393   porous medium. *Engineering Science and Technology, an International Journal*.

394 [29] Mishra, S. R., Baag, S., & Mohapatra, D. K. (2016). Engineering Science and Technology ,
395   an International Journal Chemical reaction and Soret effects on hydromagnetic micropolar
396   fluid along a stretching sheet. *Engineering Science and Technology, an International*
397   *Journal*, *19*(4), 1919–1928. https://doi.org/10.1016/j.jestch.2016.07.016

398 [30] Anwar, M. I., Shafie, S., Hayat, T., Shehzad, S. A., & Salleh, M. Z. (2017b). Numerical
399   study for MHD stagnation-point flow of a micropolar nanofluid towards a stretching sheet.
400   *Journal of the Brazilian Society of Mechanical Sciences and Engineering*, *39*(1), 89–100.
401   https://doi.org/10.1007/s40430-016-0610-y

402 [31] Khan, W. A., & Pop, I. (2010). Boundary-layer flow of a nanofluid past a stretching
403   sheet. *International journal of heat and mass transfer*, *53*(11-12), 2477-2483.

404

405

406

407

408

409

410